



Quantum diffusion regime of charge transport in GdB₆ caused by electron and lattice instabilityAlexander P. Dudka,^{1,2} Olga N. Khrykina,^{1,2} Nadezhda B. Bolotina,¹ Natalya Yu. Shitsevalova,³ Volodymyr B. Filipov,³ Mikhail A. Anisimov ,² Slavomir Gabani,⁴ Karol Flachbart,⁴ and Nikolay E. Sluchanko ^{2,5,*}¹*Shubnikov Institute of Crystallography of Federal Scientific Research Centre ‘Crystallography and Photonics’ of Russian Academy of Sciences, 59 Leninskiy Ave., 119333 Moscow, Russia*²*Prokhorov General Physics Institute, Russian Academy of Sciences, 38 Vavilov Str., 119991 Moscow, Russia*³*Frantsevich Institute for Problems of Materials Science, National Academy of Sciences of Ukraine, 3 Krzhyzhanovskyy Str., 03142 Kiev, Ukraine*⁴*Institute of Experimental Physics, Slovak Academy of Sciences, Watsonova 47, 04001 Košice, Slovak Republic*⁵*Moscow Institute of Physics and Technology (State University), 9 Institutskiy Per., 141700 Dolgoprudny, Russia*

(Received 18 April 2019; revised manuscript received 8 August 2019; published 4 November 2019)

Based on accurate x-ray structure analysis of GdB₆ over the temperature range 85–300 K it has been shown that anomalously strong charge carrier scattering in the quantum diffusion regime of charge transport in this compound arises due to the formation of (i) dynamically coupled Gd³⁺ pairs of about 3.3 Å in size and with energy of quasilocal oscillations ~7–8 meV, and due to (ii) dynamic charge stripes along the [001] direction of the cubic lattice. It has been shown that the anharmonic approximation is appropriate when analyzing the static and dynamic components of the atomic displacement parameters of gadolinium. The barrier height of double-well potential of Gd³⁺ ions was determined both from low-temperature heat capacity measurements and from the electron density distribution reconstructed from x-ray data.

DOI: [10.1103/PhysRevB.100.205103](https://doi.org/10.1103/PhysRevB.100.205103)**I. INTRODUCTION**

A short time after the discovery of high-temperature superconductivity in cuprates, it became clear that the highest critical temperatures T_c were observed in materials with a linear temperature dependence of resistivity $\rho(T)$ (see, for example, Refs. [1–5]), which could be extended to very high temperatures (~1000 K [1]) leading to violation of the Mott-Ioffe-Regel limit [6]. Later on, a similar behavior of $\rho(T)$ was found in pnictides [7,8] and organic superconductors [9,10] as well as in many heavy fermionic metals and superconductors [11,12] including those located in the vicinity of quantum critical point (QCP) [13]. Many different mechanisms were proposed to explain this effect, including quantum critical theories [13] and more exotic approaches, but its nature is the subject of active debates so far. As shown by the analysis of experimental results obtained for Sr₃Ru₂O₇ in the vicinity of QCP [14], the linear dependence of resistivity can be characterized by the same carrier scattering frequency in conductors of different classes. A single description can thus be offered in terms of diffusion transport with a diffusion coefficient that has a value close to the quantum limit $D = \hbar/m^*$, where \hbar is the Planck constant and m^* is the effective mass of charge carriers [11].

Taking into account that all the above-listed strongly correlated electronic systems (SCES) have complicated electronic and crystal structures, it is of interest to study a single-crystal conductor with a cubic crystal structure and with T -linear resistivity. Fine structure details and mechanisms of carrier

scattering, which cause the appearance of the diffusion regime of charge transport near the quantum limit, seem to be in this case the most promising for study. In this work, single crystals of gadolinium hexaboride GdB₆ with a simple cubic structure similar to that of CaB₆ [Fig. 1(a)] and a T -linear resistivity $\rho(T)$ was opted to study fine details of the crystal and electronic structure, static and dynamic components of atomic displacement parameters, and specific heat. Unlike some SCES located in the vicinity of QCP, GdB₆ is an antiferromagnetic (AF) metal (Néel temperature $T_N \approx 16$ K [15]), in which the majority of charge carriers (~70%) are nonequilibrium (hot) electrons, which participate in the formation of collective modes [16] already at room temperature. In this study it is shown that dynamically coupled Gd pairs in combination with dynamic charge stripes are formed in GdB₆ with temperature lowering [Figs. 1(b)–1(d)] and create very strong charge carrier scattering in the quantum diffusion regime.

II. EXPERIMENTAL TECHNIQUES

High-quality single crystals of GdB₆ were grown by vertical crucible-free induction melting in an argon gas atmosphere. Preparation and characterization details of rare earth (RE) higher borides used in thermal and structural studies are described elsewhere [17–20]. Heat capacity was measured on a PPMS-9 (Quantum Design, Inc.) installation; measurements of resistance were performed in a four-terminal scheme with current (I) commutation ($I \parallel [110]$, $I = 10$ –100 mA). Single-crystal x-ray data were collected with extremely high accuracy at nine temperatures in the range 85–300 K using an Xcalibur

*nes@lt.gpi.ru

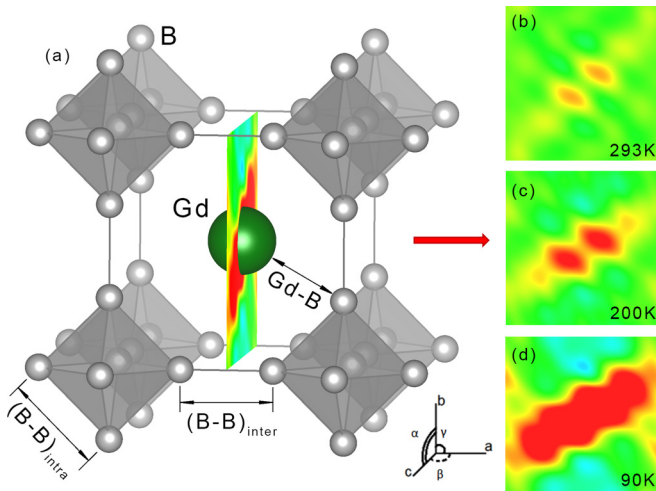


FIG. 1. (a) Unit cell of GdB₆. Difference Fourier maps of the residual electron density distribution (Δg) are shown in the (100) plane of the crystal lattice at temperatures (b) 293 K, (c) 200 K, and (d) 90 K (see text for further details).

diffractometer (Rigaku Oxford Diffraction) equipped with a charge-coupled device detector EOS S2.

III. RESULTS AND DISCUSSION

A. Resistivity and specific heat

Temperature dependences of resistivity $\rho(T)$ and specific heat $C(T)$ of GdB₆ are shown in Figs. 2(a) and 2(b), correspondingly. As in Ref. [15], a linear $\rho(T)$ dependence is observed here in the range of 30–300 K. At $T_N \approx 16$ K strong anomalies are observed, which are associated with the AF transition. In Fig. 2(a) also similar data for the nonmagnetic reference compound LaB₆ are presented, whose resistivity is 4–30 times lower than that of GdB₆. The comparison

of low-temperature heat capacity curves [Fig. 2(b)] in the paramagnetic phase of GdB₆ and in diamagnetic LaB₆ leads to conclusions about significant differences that may be related, as Gd ions have no orbital momentum ($s = 7/2$, $l = 0$ for Gd³⁺), to markedly different frequencies of quasilocal vibrations of La³⁺ and Gd³⁺ ions. The boron sublattice of these two RE hexaborides gives equal Debye contributions C_D to heat capacity (their Debye temperature is $\theta_D = 1160$ K, Fig. 2(c) and Ref. [17]), while the Einstein contributions C_E from the RE ions are significantly different corresponding to Einstein temperatures $\theta_E(\text{LaB}_6) = 140$ K [17,21,22] and $\theta_E(\text{GdB}_6) = 91$ K [23] [Fig. 2(d)]. For GdB₆, additionally to the huge anomaly at $T_N \approx 16$ K, we detect also a large-amplitude Schottky component C_{Sch} [Fig. 2(e)] that corresponds to a barrier height of $\Delta E \approx 37$ K in the double-well potential (DWP). It is worth noting that the Schottky contribution is about three orders of magnitude higher than it may be estimated from any possible magnetic anomaly caused by isolated Gd ions. Therefore, it should be attributed to magnetovibrating states of Gd pairs (see below) located in the DWPs.

B. Crystal structure

The structure of GdB₆ was refined in the cubic $Pm - 3m$ group at nine temperatures within 85–300 K in the harmonic approximation of atomic vibrations. A unit cell of GdB₆ is presented in Fig. 1(a). The central Gd atom is surrounded by eight B₆ octahedra situated at vertexes of the cubic lattice. Temperature dependent interatomic distances Gd-B, (B-B)_{intra} in an octahedron and (B-B)_{inter} between octahedra are presented in Fig. 3(a).

The lattice parameters were additionally refined without symmetry-induced constraints in order to assess the degree and character of Jahn-Teller distortions. Temperature dependences of linear and angular lattice parameters are given in

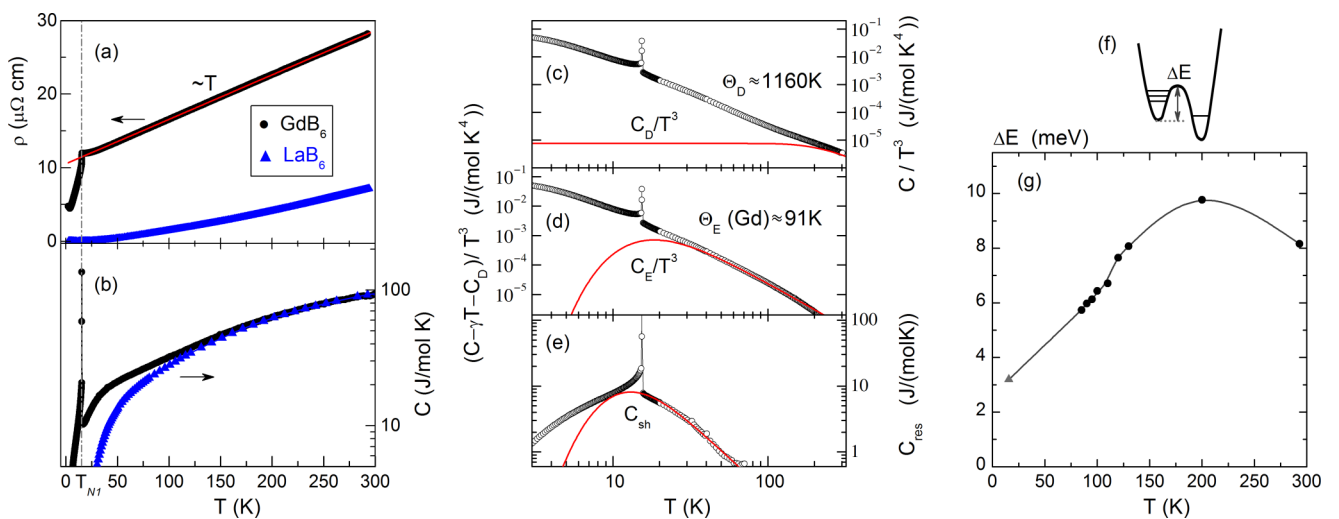


FIG. 2. Temperature dependences of (a) resistivity and (b) specific heat in GdB₆. For comparison, data obtained for the nonmagnetic reference compound LaB₆ are also shown. The straight line approximates the linear part of the resistance curve in the range of 30–300 K. Different contributions to heat capacity: (c) the Debye contribution C_D ; (d) the Einstein contribution C_E ; (e) the low temperature Schottky component C_{Sch} . Panels (f)–(g) show (f) a schematic view of the double-well potential with a barrier height ΔE and (g) the temperature dependence of barrier height derived from the heat capacity (triangle) and x-ray (circles) experiments.

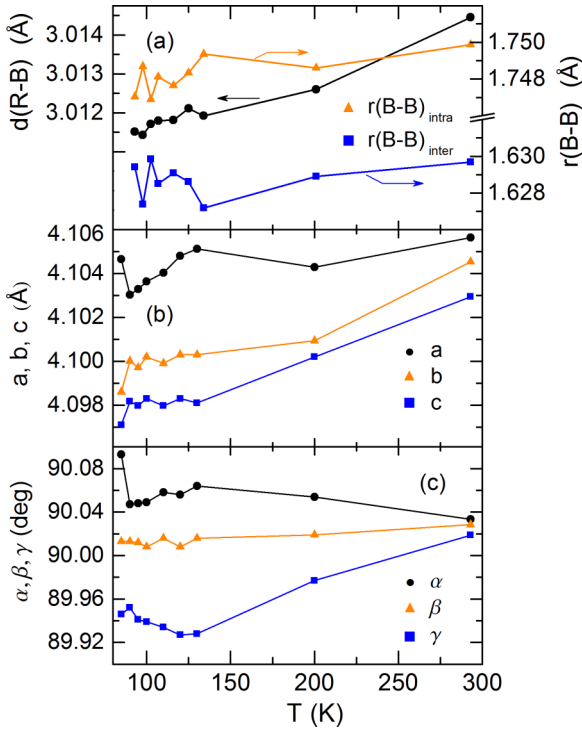


FIG. 3. (a) Temperature dependences of interatomic distances Gd-B, (B-B)_{intra} within B₆ octahedra and (B-B)_{inter} between boron octahedra in the cubic lattice of GdB₆. Temperature dependences of symmetry-independent lattice parameters *a*, *b*, *c* (b) and angles α , β , γ (c) of the GdB₆ crystal structure. The error bars do not exceed the size of experimental symbols.

Figs. 3(b) and 3(c), respectively [see labeling in Fig. 1(a)]. It can be seen that differences in lattice periods and angles, although very small, remain over the whole temperature range indicating violations of cubic symmetry, previously observed in dodecaboride LuB₁₂ [24]. Since trigonal distortions of the LuB₁₂ lattice are highly likely to be the key factors determining the occurrence of dynamic charge stripes in higher borides, it is of interest to analyze difference Fourier maps of GdB₆ for possible symmetry violations as it was done in the case of LuB₁₂. The Fourier synthesis of electron density (ED) does not require information on crystal symmetry as

it is based on reflection intensities and atomic coordinates. This allows the analysis of fine crystal structure details on symmetry-independent difference Fourier maps [18,19,24]. Visible (100), (010), and (001) faces of each cube in panels (a)–(c) of Fig. 4 contain Gd³⁺ ions in vertexes of the unit cells. For easier viewing of the filamentary structure of residual ED at temperatures 293, 200, and 90 K each cube in Fig. 4 consists of eight unit cells. Different values of residual ED (Δg) within the layer are represented in Fig. 4 by different colors (Δg acquires values $0.05(e \text{ \AA}^{-3}) < \Delta g < 0.8\Delta g_{\text{max}}$). This allows us to visualize two characteristic properties: (1) already at room temperature, at distances of about $\pm 0.5 \text{ \AA}$ from the Gd site, and approximately in the direction of the face diagonal of the unit cell, ED maxima predicting the formation of Gd-Gd pairs are observed; (2) with temperature decrease, the amplitude of maxima increases significantly, and the observed maxima stretch into stripes, simultaneously turning approximately into the [0-13] direction in the (100) plane [Fig. 4(c)]. As a result, zigzag shaped charge stripes are formed at low temperatures near the (100) plane, which are mainly oriented along the *c* axis [Fig. 4(c)]. Residual ED distributions in the (100) plane of a single cell are shown in Figs. 1(b)–1(d) with an origin shifted by $(\frac{1}{2}, \frac{1}{2}, \frac{1}{2})$ as compared to Fig. 4. It should be emphasized that in the presence of cubic lattice distortions, e.g., of boron vacancies [17,22] and of structure disorder due to isotopic ¹⁰B-¹¹B substitutions in the boron sublattice (natural isotope distribution is 18.8% ¹⁰B and 81.2% ¹¹B), the formation of selected direction along charge stripes leads to the appearance of uniaxial anisotropy in these cubic crystals.

Evidently, the appearance of additional ED at distances of about $\pm 0.5 \text{ \AA}$ from the Gd site should be analyzed in terms of double-well potentials and anharmonic vibrations of Gd ions. The one-particle potential $V^{\text{OPP}}(\mathbf{u})$ in a point distant by vector \mathbf{u} from a selected atom can be estimated from the formula [25]:

$$V^{\text{OPP}}(\mathbf{u}) = -k_{\text{B}}T\{\ln G(\mathbf{u}) - \ln G(\mathbf{u} = 0)\}, \quad (1)$$

where $G(\mathbf{u})$ is the generalized atomic probability density function. In our work, pseudopotential curves were drawn along stripes in the (100) plane at each of nine temperatures using formula (1) with symmetry-independent ED values of $G(\mathbf{u})$ instead of symmetry-restricted values of $G(\mathbf{u})$ in order to

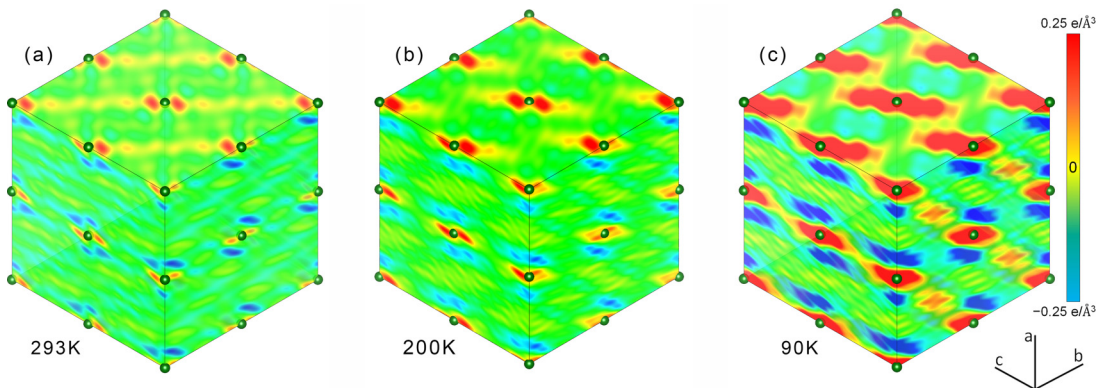


FIG. 4. Different Fourier maps of residual ED distribution (Δg) at temperatures (a) 293 K, (b) 200 K, and (c) 90 K in three orthogonally related planes {100} of the crystal lattice passing through Gd atoms. Three blocks of eight unit cells are shown for easier viewing of ED (electron density) filamentary structures.

estimate the barrier heights $\Delta E(T)$ in the DWP of Gd^{3+} ions. The legality of such a replacement is discussed in Ref. [25]. Calculated from x-ray data the $\Delta E(T)$ dependence is presented in Fig. 2(g) where the DWP barrier height obtained from heat capacity measurements is also shown for comparison. The tendency to a decrease of $\Delta E(T)$ below 8 meV with temperature lowering in the range 20–200 K [Fig. 2(g)] is in accordance with the softening of Gd quasilocal mode observed in Refs. [26,27] by inelastic x-ray scattering. On the other hand, authors of Refs. [26,27] found that the L mode (the phonon branch propagating along the [110] axis) softened only by 9% from 300 down to 20 K. For the longitudinal phonon mode along the [100] direction in GdB_6 a softening of about 13% was detected taking the phonon energy value $E_{\text{ph}} \sim 5.7$ meV at 20 K [28]. Besides, it was concluded in Ref. [28] that the phonon softening behavior was strongly anisotropic, indicating an anharmonic or shallow potential for Gd ions. It is worth noting that Raman scattering results [29,30] also indicate that the anharmonicity of the RE mode is anisotropic, that is, it depends on the vibrating and propagating directions of the RE mode in GdB_6 . As follows from difference ED maps, the most significant softening is developed in the [0-13] direction of the (100) plane which corresponds to the configuration of dynamic charge stripes in GdB_6 [Fig. 4(c)]. Actually, the structural diffraction experiment does not distinguish between dynamic and static atomic displacements; therefore, on maps of Fourier syntheses, both dynamic and static effects look the same. But, if pairs were stable/static, it would give weak reflexes from lattice interstices. But, we did not find such reflexes, despite that we observe a fairly good statistics of quantum counting. Therefore, we need to choose the case of dynamic atomic displacements, which means that the Gd^{3+} ions move in a double-well potential. This looks natural for loosely bound state of Gd ions embedded in large size B_{24} cuboctahedrons of the RB_6 lattice and taking into account large amplitude atomic displacements. Within this quantum motion of heavy rare earth ions towards each other when “hanging” in extreme positions, corresponding Gd pairs appear temporarily in the hexaboride lattice.

C. Dynamic and static atomic displacements

Atomic displacement parameters are components of the Debye-Waller factor $T(\mathbf{H})$ that describe the atomic distribution near the lattice points being a part of the structure factor $F(\mathbf{H})$ [31]. Harmonic vibrations are represented by the factor $T_{\text{harm}}(\mathbf{H}) = \exp(-2\pi^2 U^{ij} a^i a^j h_i h_j)$, where U^{ij} is a second-rank tensor; a^i , a^j and h_i , h_j , $1 \leq i, j \leq 3$, are, respectively, periods of reciprocal lattice and Miller indexes. An anharmonicity of atomic motion is accounted, if necessary, by an expansion of $T(\mathbf{H})$ into the Gram-Charlier series with tensor coefficients of rank higher than two. The second-rank U^{ij} tensor can be written in the form of symmetric matrix $\{u_{ij}\}$ whose diagonal elements define the equivalent mean-square atomic displacement $u_{\text{eq}} = (u_{11} + u_{22} + u_{33})/3$, also in the case when $T(\mathbf{H})$ contains additional higher-rank tensors [31].

Difference ED (Δg) Fourier maps [31] shown above (in Fig. 4) were built for the GdB_6 crystal structure refined in the harmonic approximation of atomic vibrations (in fact, harmonic vibrations of Gd in special position $4a$ of the

$Fm\bar{3}m$ group are isotropic), so that any asymmetry of the ED distribution could be well seen. Gd atoms loosely bound with boron cages and located in large size cavities of the rigid covalent boron framework (the radius of B_{24} cavity ($\sim 2 \text{ \AA}$) exceeds considerably the Gd ionic radius $r(\text{Gd}) \approx 0.94 \text{ \AA}$ [23]) are usually considered as independent harmonic oscillators. This allows us to fit the temperature-dependent parameters (displacements) $u_{\text{eq}}(\text{Gd})$ and $u_{\text{eq}}(\text{B})$ by Einstein (2) and Debye (3) formulas, respectively,

$$u_{\text{eq}}(\text{Gd}) = \frac{h^2}{4\pi^2 k_B m_a \theta_E} \left(\frac{1}{2} + \frac{1}{\exp(\frac{\theta_E}{T}) - 1} \right) + \langle u^2 \rangle_{\text{shift}}(\text{Gd}), \quad (2)$$

$$u_{\text{eq}}(\text{B}) = \frac{3h^2}{4\pi^2 k_B m_a \theta_D} \times \left(\frac{1}{4} + \left(\frac{T}{\theta_D} \right)^2 \int_0^{\frac{\theta_D}{T}} \frac{y}{\exp(y) - 1} dy \right) + \langle u^2 \rangle_{\text{shift}}(\text{B}), \quad (3)$$

where h , k_B are Planck and Boltzmann constants, m_a is the atomic mass, θ_E and θ_D are the Einstein and Debye temperatures, and $\langle u^2 \rangle_{\text{shift}}$ is the static mean-square displacement. As can be seen from Figs. 3(b) and 3(c), the lattice deviations from cubic, albeit increase with decreasing temperature, remain very small. The relative atomic coordinates and the equivalent atomic displacement parameters practically do not react to such small changes, therefore “cubic” values of u_{eq} can be always taken into the fitting. Reducing symmetry only complicates the structural model, but it does not affect the result of the fit. In Eqs. (2) and (3) there are two dynamic components of the equivalent atomic displacement u_{eq} that correspond to the thermal and zero-temperature vibrations of these atoms, and one static term that determines the temperature-independent shift of these atoms from their lattice sites. This static term arises mainly due to boron vacancies (the occurrence of about 1–9% of vacancies at boron sites has been detected in RB_6 [22]) and due to substitutional disorder which is present in RE hexaborides with natural (18.8% ^{10}B and 81.2% ^{11}B) boron composition.

Difference Fourier maps of residual ED (Fig. 4) accurately indicate the appearance of Gd–Gd pairs already at room temperature and this tendency increases strongly with temperature lowering. The observed result is in accordance with the dynamical Jahn-Teller (JT) model proposed by Kasuya for GdB_6 where each Gd atom distorts to a quasistable position along each [001] direction and the ground state is arranged as a linear combination of six equivalent sites keeping cubic symmetry (pair-distorted dynamic JT effect) [32]. Moreover, a detailed Raman study [29] has shown that the low frequency vibration of R ions in RB_6 cannot be regarded as an independent mode, but as a coherent mode with long-range interaction between R ions. Taking these findings into account we have developed here a model in which the role of independent oscillators is assigned to Gd–Gd pairs. The Gd–Gd components, on the contrary, lose their independence, and their displacements may be anharmonic. To test this

TABLE I. Einstein θ_E and Debye θ_D temperatures, temperature independent components of the mean-square atomic displacements $\langle u^2 \rangle_{\text{zero}}$, $\langle u^2 \rangle_{\text{shift}}$, $\langle u^2 \rangle_{\text{sum}} = \langle u^2 \rangle_{\text{zero}} + \langle u^2 \rangle_{\text{shift}}$, refined in structure models I (anharmonic for Gd and harmonic for boron) and II (harmonic both for Gd and B); R – approximation accuracy.

Model (atoms)	θ_E/θ_D (K)	$\langle u^2 \rangle_{\text{zero}}$ (\AA^2)	$\langle u^2 \rangle_{\text{shift}}$ (\AA^2)	$\langle u^2 \rangle_{\text{sum}}$ (\AA^2)	R (%)
I (B)	- / 1206 ± 48	0.0028	0.0020	0.0048	1.38
I (Gd-Gd)	79 ± 3 / -	0.00098	0.00906	0.01004	1.62
II (Gd)	90 ± 1 / -	0.00171	0.00050	0.00221	1.02

hypothesis, we have refined the structure of GdB_6 at nine temperatures, taking into account the anharmonicity of Gd ions up to the sixth order (model I). The previous harmonic model was named as model II for comparison. The values of $u_{\text{eq}}(\text{Gd})$ from model I were assigned to $u_{\text{eq}}(\text{Gd-Gd})$ of atomic pairs and substituted into Eq. (2) together with doubled atomic mass $2m_a(\text{Gd-Gd})$ to estimate the Einstein temperature. A similar estimation was done for model II using corresponding to $u_{\text{eq}}(\text{Gd})$ and a single atomic mass $m_a(\text{Gd})$. The resulting $u_{\text{eq}}(\text{B})$ values were almost equal for both models. Those from model I were then substituted into Eq. (3) to estimate the Debye temperature.

The set of parameters deduced by the analysis based on Eqs. (2) and (3) in models I and II is presented in Table I. It contains values of θ_E and θ_D as well as zero temperature atomic vibrations $\langle u^2 \rangle_{\text{zero}}$ obtained from Eqs. (2) and (3) at $T = 0$, static components $\langle u^2 \rangle_{\text{shift}}$, and the sum of temperature independent components $\langle u^2 \rangle_{\text{sum}} = \langle u^2 \rangle_{\text{shift}} + \langle u^2 \rangle_{\text{zero}}$. As can be seen from Table I, the refined value of the Debye temperature $\theta_D(\text{I}) = 1206 \pm 48$ K coincides within the limits of accuracy with $\theta_D = 1160$ K derived from heat capacity measurements [Fig. 2(c)]. The Einstein temperature $\theta_E(\text{I}) \approx 80$ K determined on the assumption of Gd-Gd pairs is less than $\theta_E(\text{II}) \approx 90$ K but, in general, it corresponds to the energy of 7–8 meV of the Gd quasilocal mode found in [26–28]. For Gd ions in model I, the contribution of the static component to the temperature independent atomic displacement parameter $\langle u^2 \rangle_{\text{sum}}$ is an order of magnitude higher than that of $\langle u^2 \rangle_{\text{zero}}$, while both these contributions are almost equal for the B atoms. Moreover, in the case of vibrationally coupled Gd pairs (model I) the total (static plus dynamic) mean-square displacements of the heavy Gd atom ($m_a \approx 157$ amu) exceed significantly those of the light B atom ($m_a \approx 11$ amu) [Figs. 5(a) and 5(b)]. The same situation was discussed in detail in Ref. [22] where the inequality $u_{\text{eq}}(\text{B}) < u_{\text{eq}}(\text{R})$ was found to be valid for all studied RE hexaborides ($R = \text{La, Ce, Pr, Nd, Sm, Gd, Eu}$).

D. Electronic and lattice instability in GdB_6

When discussing the nature of (i) large amplitude atomic displacements in GdB_6 , (ii) the formation of dynamically coupled Gd-Gd pairs and (iii) the appearance of dynamic charge stripes at low temperatures observed in this study, it is worth noting also the recent results of dynamic conductivity investigation of $\text{Gd}_x\text{La}_{1-x}\text{B}_6$ [16]. In particular, it has been found in Ref. [16] that there are two components in the

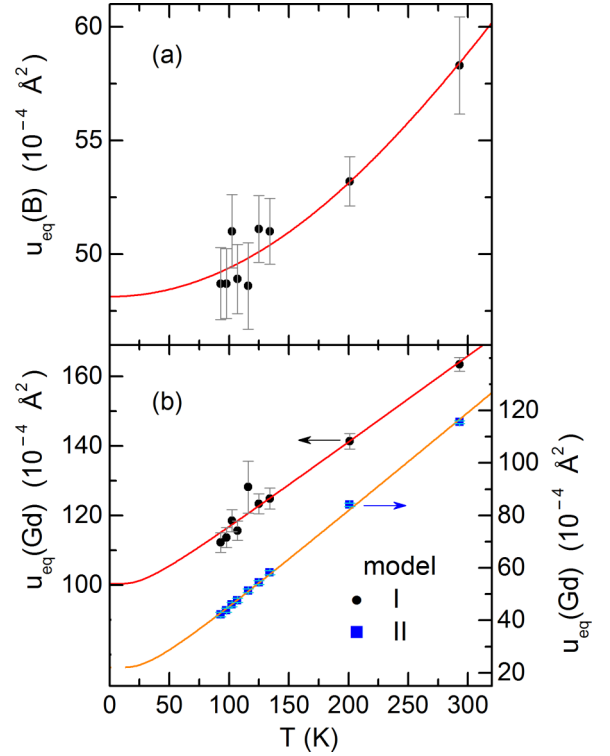


FIG. 5. Temperature dependences of the mean-square atomic displacements for (a) boron U_B and (b) Gd cation U_{Gd} as obtained from models I (Gd-Gd atomic pairs) and II (single Gd ions) (see text for details).

dynamic conductivity spectra, and, additionally to the contribution from Drude electrons a strong collective mode has been observed with a frequency of ~ 1000 cm^{-1} and with a damping of 2200 cm^{-1} (overdamped oscillator), which includes up to 70% of the conduction electrons available in these metals. The collective mode is typical for systems with cooperative dynamic JT effect in boron clusters [20,33] and in the case of GdB_6 it results from the JT instability of B_6 molecules (clusters). In this scenario the cooperative high-frequency JT boron vibrations cause rattling modes of Gd^{3+} ions, which are quasilocal low-frequency vibrations (Einstein mode). This Einstein mode is characterized by a very large vibration amplitude that leads to strong variation of the $5d$ - $2p$ hybridization of electronic states of Gd and boron ions. According to results of band structure calculations for RE hexaborides [34–36] both the Gd $5d$ and B $2p$ states contribute to the conduction band. Thus, the modulation of the conduction band produces “hot charge carriers”, which in turn are strongly scattered on the Gd quasilocal mode. With the temperature lowering, these oscillating hot electrons in GdB_6 form a filamentary structure (dynamic charge stripes), which is detected in present study and shown on the ED maps of Fig. 4. As shown in Fig. 4, a structure of nanometer size ac-conducting channels is formed at low temperatures in the (100) plane of GdB_6 . The channels are oriented approximately in the [001] direction and they are accompanied with the formation of vibration-coupled Gd pairs. As a result, the strongest charge carriers scattering in GdB_6 is due to (i) the boron sublattice JT instability and (ii) the appearance of the nonequilib-

rium (hot) electrons which are involved in the high frequency (~ 240 GHz [33]) quantum motion highlighted in dynamic charge stripes.

IV. CONCLUSION

Fine details of the crystal and electronic structure have been studied in combination with features of the atomic dynamics in GdB_6 , a compound with a simple cubic structure, which is located in vicinity of the quantum diffusion regime of charge transport and that demonstrates a wide range linear temperature dependence of resistivity. As a result of high-precision x-ray diffraction studies of high-quality GdB_6 single crystals in the temperature range 85–300 K, it has been shown that already at room temperature Gd^{3+} ions combine into dynamically coupled Gd-Gd pairs. With decreasing temperature the emergence of dynamic charge stripes is observed in the vicinity of (100) planes. These stripes form a nanometer size filamentary structure of ac-conducting channels in the [001] direction. It has been concluded that just these two factors (formation of Gd-Gd pairs and charge stripes) representing the lattice and electron instabilities are responsible for the extremely strong charge carrier scattering, which leads to the

diffusion regime of charge transport in GdB_6 . The size of the Gd-Gd pairs was estimated to be ~ 3.3 Å, and the variation of the barrier height in the double-well potential is within the 3–8 meV limit.

ACKNOWLEDGMENTS

This work was supported by the Russian Ministry of Science and Higher Education within the State assignment FSRC ‘Crystallography and Photonics’ Russian academy of Science (RAS) in part of methodological developments for x-ray data processing and by the Russian Science Foundation, Project No. 17-12-01426, in part of studying the structure and properties of GdB_6 crystals. X-ray diffraction data were collected using the equipment of the Shared Research Center FSRC ‘Crystallography and Photonics’ of RAS and was supported by the Russian Ministry of Education and Science (project RFMEFI62119X0035); measurements of heat capacity were carried out in the Center of Low Temperature Physics, Slovak Academy of Sciences. The work of K.F. and S.G. was supported by the Slovak agencies VEGA (Grant No. 2/0032/16) and APVV (Grant No. 17–0020).

-
- [1] M. Gurvitch and A. T. Fiory, *Phys. Rev. Lett.* **59**, 1337 (1987).
- [2] K. Takenaka, K. Mizuhashi, H. Takagi, and S. Uchida, *Phys. Rev. B* **50**, 6534 (1994).
- [3] Y. Ando, K. Segawa, S. Komiya, and A. N. Lavrov, *Phys. Rev. Lett.* **88**, 137005 (2002).
- [4] A. W. Tyler, Y. Ando, F. F. Balakirev, A. Passner, G. S. Boebinger, A. J. Schofield, A. P. Mackenzie, and O. Laborde, *Phys. Rev. B* **57**, R728(R) (1998).
- [5] T. Watanabe, T. Fujii, and A. Matsuda, *Phys. Rev. Lett.* **79**, 2113 (1997).
- [6] A. Ioffe and A. Regel, *Prog. Semicond.* **4**, 237 (1960).
- [7] H. Takahashi, T. Okada, Y. Imai, K. Kitagawa, K. Matsubayashi, Y. Uwatoko, and A. Maeda, *Phys. Rev. B* **86**, 144525 (2012).
- [8] M. Abdel-Hafez, J. Ge, A. N. Vasiliev, D. A. Chareev, J. Van de Vondel, V. V. Moshchalkov, and A. V. Silhanek, *Phys. Rev. B* **88**, 174512 (2013).
- [9] N. Doiron-Leyraud, S. René de Cotret, A. Sedeki, C. Bourbonnais, L. Taillefer, P. Auban-Senzier, D. Jérôme, and K. Bechgaard, *Eur. Phys. J. B* **78**, 23 (2010).
- [10] J. S. Brooks, *Rep. Prog. Phys.* **71**, 126501 (2008).
- [11] T. Hu, Y. Liu, H. Xiao, G. Mu, and Y.-F. Yang, *Sci. Rep.* **7**, 9469 (2017).
- [12] R. Daou, C. Bergemann, and S. R. Julian, *Phys. Rev. Lett.* **96**, 026401 (2006).
- [13] G. R. Stewart, *Rev. Mod. Phys.* **73**, 797 (2001).
- [14] J. A. N. Bruin, H. Sakai, R. S. Perry, and A. P. Mackenzie, *Science* **339**, 804 (2013).
- [15] H. Nozaki, T. Tanaka, and Y. Ishizawa, *J. Phys. C* **13**, 2751 (1980).
- [16] E. S. Zhukova, B. P. Gorshunov, G. A. Komandin, L. N. Alyabyeva, A. V. Muratov, Yu. A. Aleshchenko, M. A. Anisimov, N. Yu. Shitsevalova, S. E. Polovets, V. B. Filipov *et al.*, *Phys. Rev. B* **100**, 104302 (2019).
- [17] M. A. Anisimov, V. V. Glushkov, A. V. Bogach, S. V. Demishev, N. A. Samarin, S. Yu. Gavrilkin, K. V. Mitsen, N. Yu. Shitsevalova, A. V. Levchenko, V. B. Filipov *et al.*, *JETP* **116**, 760 (2013).
- [18] N. Sluchanko, A. Bogach, N. Bolotina, V. Glushkov, S. Demishev, A. Dudka, V. Krasnorussky, O. Khrykina, K. Krasikov, V. Mironov *et al.*, *Phys. Rev. B* **97**, 035150 (2018).
- [19] N. B. Bolotina, A. P. Dudka, O. N. Khrykina, V. N. Krasnorussky, N. Yu. Shitsevalova, V. B. Filipov, and N. E. Sluchanko, *J. Phys.: Condens. Matter* **30**, 265402 (2018).
- [20] N. E. Sluchanko, A. P. Dudka, O. N. Khrykina, N. B. Bolotina, A. N. Azarevich, A. V. Bogach, S. Yu. Gavrilkin, S. V. Demishev, A. V. Dukhnenko, N. Yu. Shitsevalova *et al.*, *JETP Lett.* **108**, 691 (2018).
- [21] D. Mandrus, B. C. Sales, and R. Jin, *Phys. Rev. B* **64**, 012302 (2001).
- [22] M. Korsukova, in *Proceedings of the 11th International Symposium on Boron, Borides, and Related Compounds, 22-26 August 1993, Tsukuba (Japan)*, edited by R. Uno and I. Higashi (Japanese Journal of Applied Physics, Tokyo, 1994), p. 15.
- [23] Y. Takahashi, K. Ohshima, F. P. Okamura, S. Otani, and T. Tanaka, *J. Phys. Soc. Jpn.* **68**, 2304 (1999).
- [24] N. B. Bolotina, A. P. Dudka, O. N. Khrykina, V. V. Glushkov, A. N. Azarevich, V. N. Krasnorussky, S. Gabani, N. Yu. Shitsevalova, A. V. Dukhnenko, V. B. Filipov *et al.*, *J. Phys. Chem. Solids* **129**, 434 (2019).
- [25] W. F. Kuhs, *Acta Crystallogr. A* **48**, 80 (1992).
- [26] K. Iwasa, R. Igarashi, K. Saito, C. Laulhe, T. Orihara, S. Kunii, K. Kuwahara, H. Nakao, Y. Murakami, F. Iga *et al.*, *Phys. Rev. B* **84**, 214308 (2011).
- [27] K. Iwasa, F. Iga, A. Yonemoto, Y. Otomo, S. Tsutsui, and A. Q. R. Baron, *J. Phys. Soc. Jpn.* **83**, 094604 (2014).
- [28] K. Iwasa, R. Igarashi, K. Saito, C. Laulhe, T. Orihara, S. Kunii, K. Kuwahara, H. Nakao, Y. Murakami, F. Iga *et al.*, *Chinese J. Phys.* **49**, 231 (2011).

- [29] N. Ogita, S. Nagai, N. Okamoto, M. Udagawa, F. Iga, M. Sera, J. Akimitsu, and S. Kunii, *Phys. Rev. B* **68**, 224305 (2003).
- [30] N. Ogita, T. Hasegawa, M. Udagawa, F. Iga, and S. Kunii, *J. Phys.: Conf. Ser.* **176**, 012032 (2009).
- [31] See Supplemental Material at <http://link.aps.org/supplemental/10.1103/PhysRevB.100.205103> for (a) account of anharmonicity in atomic motion, (b) Fourier synthesis of ED, and (c) resistivity analysis.
- [32] T. Kasuya, *J. Magn. Magn. Mater.* **174**, L28 (1997).
- [33] N. Sluchanko, A. N. Azarevich, A. V. Bogach, N. B. Bolotina, V. V. Glushkov, S. V. Demishev, A. P. Dudka, O. N. Khrykina, V. B. Filipov, N. Yu. Shitsevalova *et al.*, *J. Phys.: Condens. Matter* **31**, 065604 (2019).
- [34] Y. Kubo, S. Asano, H. Harima, and A. Yanase, *J. Phys. Soc. Jpn.* **62**, 205 (1993).
- [35] A. E. Baranovskiy, G. E. Grechnev, V. D. Fil, T. V. Ignatova, A. V. Logosha, A. S. Panfilov, I. V. Svechkarev, N. Yu. Shitsevalova, V. B. Filipov, and O. Eriksson, *J. Alloys Compd.* **442**, 228 (2007).
- [36] L. Xiao, Y. Su, J. Ran, Y. Liu, W. Qiu, J. Wu, F. Lu, F. Shao, D. Tang, and P. Peng, *J. Appl. Phys.* **119**, 164903 (2016).